J Sci Comput (2012) 52:519–545
DOI 10.1007/s10915-011-9557-4

P_1-Nonconforming Quadrilateral Finite Volume Methods for the Semilinear Elliptic Equations

Xinlong Feng · Rongfei Li · Yinnian He · Demin Liu

Received: 2 April 2011 / Revised: 6 October 2011 / Accepted: 4 November 2011 /
Published online: 19 November 2011

Abstract In this paper we use P_1-nonconforming quadrilateral finite volume methods with interpolated coefficients to solve the semilinear elliptic problems. Two types of control volumes are applied. Optimal error estimates in H^1-norm on the quadrilateral mesh and superconvergence of derivative on the rectangular mesh are derived by using the continuity argument, respectively. In addition, numerical experiments are presented adequately to confirm the theoretical analysis and optimal error estimates in L^2-norm is also observed obviously. Compared with the standard Q_1-conforming quadrilateral element, numerical results of the proposed finite volume methods show its better performance than others.

Keywords Semilinear elliptic equations · Finite volume methods · P_1-nonconforming quadrilateral element · Q_1-conforming quadrilateral element · Superconvergence

1 Introduction

Finite volume methods (FVM) is an important and commonly used method for solving many practical problems in scientific and engineering computations. It is also known as the Marker-and-Cell methods [9, 15], the generalized difference methods [23, 45], finite volume element methods (FVEM) [4–6, 26, 43], covolume methods [10–12] or box methods

X. Feng · R. Li · Y. He (✉) · D. Liu
College of Mathematics and Systems Science, Xinjiang University, Urumqi 830046, P.R. China
e-mail: heyn@mail.xjtu.edu.cn

X. Feng
e-mail: fxlmath@gmail.com

R. Li
e-mail: lirongfei2008@126.com

D. Liu
e-mail: mathldm@yahoo.cn

Y. He
Faculty of Science, Xi'an Jiaotong University, Xi'an 710049, P.R. China

[2, 14, 35]. Its main virtues are the local conservation and the capability of discretizing domains with complex geometry. In general, it represents the conservation of a quantity of interest, such as mass, momentum or energy in fluid mechanics. The integral formulation of a finite volume scheme for a problem is obtained by integrating the problem over a control volume or a dual element. In fact, FVM might be regarded as a special class of Petrov-Galerkin methods where the trial function spaces are connected with the test function spaces associated with the dual partitions induced by the control volumes [21, 42]. Usually, we use different polynomial functions as trial and test spaces over the original partition and its dual partition, respectively. It is different from the standard finite element methods (FEM) which only use simple polynomial function spaces over the original partition. Although FEM is flexible to deal with the complex domains and various boundary conditions, and the theory on the convergence and stability of FEM is well established, the main drawback of FEM might be the loss of the local conservation property which can be fundamental for the simulation of many physical models, e.g., in computational fluid dynamics, hyperbolic equations, heat transfer and modeling of fuel cells [9, 15, 19, 23, 44]. Of course, one of the main limitation of FVM is the low order approximation. For most existing FVM, the test space is either a piecewise constant or a linear finite element spaces.

In this paper we shall devote ourself to study the semilinear elliptic problems by using FVM and FEM, respectively. Now a lot of numerical methods have been proposed and developed to solve the semilinear problems. Among them, FEM with interpolated coefficients is an effective and excellent method. In 1980, this method was introduced and analyzed firstly for the semilinear parabolic problems by Zlamal [46]. Later, Larson, Thomee and Zhang [22] studied the semidiscrete linear triangular FEM with interpolated coefficients, and Chen, Larson and Zhang [8] derived almost optimal order convergence on a uniform triangular mesh by using the piecewise linear finite element space and superconvergence techniques. Xiong and Chen [37–39] studied the superconvergence of triangular quadratic FEM for the nonlinear ordinary differential equation and the Q_1-conforming rectangular FEM with interpolated coefficients for the semilinear elliptic problem, respectively. Recently Xiong and Chen [40, 41] put the interpolation idea into FVEM for solving two-point boundary value problem of the semilinear differential equations and studied the Q_1-conforming rectangular FVEM with interpolated coefficients for the semilinear elliptic equation.

On the quadrilateral mesh, Li and Li [24] studied the generalized difference methods for the Poisson equation under some assumptions on the regularity of solutions and restrictions on the quadrilateral subdivision of a convex polygon domain. Zhu and Li [45] obtained a superconvergence result of the generalized difference methods in a discrete norm. Wang [36] constructed a mixed FVEM based on the rectangular mesh for the biharmonic equations by using Q_1-conforming element.

In 2003, Park and Sheen [34] introduced the nonparametic P_1-nonconforming quadrilateral FEM to solve the second-order elliptic problems independently by a novel approach. Unlike the usual conforming and nonconforming quadrilateral elements, their element only consists of piecewise linear polynomials that are continuous at the midpoints of edges. One of the benefits of using this element is convenient to use the rectangular or quadrilateral mesh with much less degrees of freedom than the usual quadrilateral nonconforming elements. Note that for Q_1-conforming quadrilateral element, they have the same degrees of freedom for different boundary conditions. On the other hand, from different points of view, the different P_1-nonconforming quadrilateral finite element can also be found in some references, e.g. the RQC4 element proposed in [44] (has been published 20 years ago). Furthermore, motivated by references [33, 34, 44], the parametric constrained nonconforming rotated Q_1 element are presented in [20] and the nonconforming double set parameter rotated Q_1 element are also presented in [28–32]. In 2006, Mao, Chen and Sun [31] presented

a four-parameter quadrilateral nonconforming element with double set parameter by using different motivation and ideas (It is originated from the nonconforming rotated Q_1 element and bilinear element, they call it QB element) and proved that it is an anisotropic and superconvergent nonconforming quadrilateral element. Note that QB element is equivalent to P_1-nonconforming quadrilateral element [34] under the rectangular meshes.

Later, Man and Shi [27] studied FVEM of P_1-nonconforming quadrilateral element for the elliptic problems based on a dual partition of overlapping type and obtain optimal error estimates under additional assumptions on the source term and the partition. Moreover, Grajewski, Hron and Turek [18] examined in detail the numerical behavior of Park-Sheen element with special emphasis on the treatment of Dirichlet boundary conditions and made several numerical examples for the P_1-nonconforming FEM on the quadrilateral meshes. Recently, Feng, Kim, Nam and Sheen [16] used the locally stabilized P_1-nonconforming quadrilateral and hexahedral FEM to solve the Stokes equations and obtained optimal error estimate for velocity and pressure. In this paper, we shall use P_1-nonconforming quadrilateral element to solve the semilinear elliptic problems by FVM and FEM on the rectangular mesh, respectively. Furthermore, we apply Q_1-conforming quadrilateral element to the same problems by FVM and FEM, respectively.

The outline of this paper is organized as follows. In Sect. 2, we shall introduce the FVM with interpolated coefficients and two types of control volumes for the semilinear elliptic equations. In Sect. 3, we will give preliminaries and some lemmas. In Sect. 4, we derive optimal error estimate in H^1-norm on the quadrilateral mesh. Next we will prove superconvergence of derivative on the rectangular mesh in Sect. 5. The theoretical results are investigated in detail by numerical experiments. In addition, numerical comparisons of the standard Q_1-conforming quadrilateral FVM (or FEM) and P_1-nonconforming quadrilateral FVM (or FEM) are presented in Sect. 6. Finally, conclusions are given in Sect. 7.

2 FVM with Interpolated Coefficients

Now we consider the following second order semilinear elliptic equation

$$-\Delta u + f(u) = g, \quad \text{in } \Omega \subset R^2 \tag{1}$$

with homogenous boundary condition of Dirichlet type, i.e., $u|_{\partial\Omega} = 0$ and $g \in L^2(\Omega)$. Assume that $f'(s) > 0$ for $s \in (-\infty, +\infty)$ and $f''(s)$ is continuous with respect to s, and $\Omega = (0, 1) \times (0, 1)$.

Finite volume approximations rely on the local conservation property expressed by the differential equation. Namely, integrating equation (1) over any control volume $V \subset \Omega$ with piecewise smooth boundary ∂V and using the Green formula, we obtain

$$-\int_{\partial V} \frac{\partial u}{\partial n} ds + \int_V f(u) dx dy = \int_V g dx dy, \quad \forall V \subset \Omega, \tag{2}$$

where n denotes the unit exterior normal to ∂V . The FVM of problem (2) consists of replacing the exact solution u by the finite-dimensional space of piecewise smooth functions and using a finite set of control volumes. In this paper, we shall use the rectangular partition of Ω and the piecewise linear interpolation with interpolated coefficients for u firstly.

Given a quasi-uniform rectangular partition T_h for Ω, and the nodes are (x_i, y_j), $i = 0, 1, 2, \ldots, N_x$, $j = 0, 1, 2, \ldots, N_y$. Denote $h_{x_i} = x_i - x_{i-1}$, $i = 1, 2, \ldots, N_x$, $h_{y_j} = y_j - y_{j-1}$, $j = 1, 2, \ldots, N_y$, and $h = \max_{i,j}\{h_{x_i}, h_{y_j}\}$. For any rectangular element $\tau_{ij} =$

$[x_{i-1}, x_i] \times [y_{j-1}, y_j] \in T_h$, let $Z_h(\tau_{ij})$ and $E_h(\tau_{ij})$ be the set of nodes and sides of τ_{ij} respectively. Setting $Z_h = \bigcup_{\tau_{ij} \in T_h} Z_h(\tau_{ij})$ and $E_h = \bigcup_{\tau_{ij} \in T_h} E_h(\tau_{ij})$. Further let Z_h^{in} and E_h^{in} be the set of interior nodes and sides of T_h respectively. We denote the set of all middle point of sides $e \in E_h$ (or E_h^{in}) with each node z_j by M_h (or M_h^{in}), and denote the subset of E_h consisting of those sides that have z_j is a endpoint of sides e by $E_h(j)$. Moreover, we denote the set of midpoints of sides $e \in E_h(j)$ by $M_h(j)$. In what follows, we use τ with or without subscripts to denote a element, possibly different at different occurrences in this paper, that may be a rectangular element, a trapezoidal element or a quadrilateral element.

Now we introduce P_1-nonconforming quadrilateral finite element space [34] and dual partition T_h^* associated with the quadrilateral partition T_h. Setting

$$S_h = \left\{ v_h : \Omega \to R : v_h|_\tau \in P_1(\tau) \text{ for all } \tau \in T_h \text{ and } v_h \text{ is continuous at every } m_i \in M_h^{in} \right\},$$

$$S_{0h} = \left\{ v_h \in S_h | v_h(m_i) = 0 \text{ for any } m_i \in M_h \setminus M_h^{in} \right\},$$

where $P_1(\tau) = \text{span}\{1, x, y\}$. Let $\phi_j \in S_{0h}$ be such that

$$\phi_j(m) = \begin{cases} 1, & \text{if } m \in M_h(j), \\ 0, & \text{if } m \in M_h \setminus M_h(j). \end{cases}$$

It is pointed out that if T_h is decomposed into parallelograms, ϕ_j is continuous at z_j for all j. However, ϕ_j may not be continuous in general. Under the assumption that each interior edge has at least one interior vertex as its endpoint, all functions associated with the interior nodes Z_h^{in} form the basis of S_{0h}.

Next we define a control volume V_{z_j} of node $z_j \in Z_h^{in}$, which includes z_j and four midpoints of $M_h(j)$. For boundary nodes, their control volumes should be modified correspondingly. All the control volumes constitute the dual partition T_h^*. In this paper we only consider two types of dual partitions. One is the nonoverlapping rectangular control volumes of interior vertices, and it is shown in the left subfigure of Fig. 1. The other is the overlapping quadrilateral control volumes of interior vertices which consist of four diagonals, and it is so called diagonal box [35] and shown in the right subfigure of Fig. 1.

Remark 2.1 Moreover, we consider a trapezoidal mesh in Fig. 2 which appear in [16, 20] and two types of control volumes in Fig. 3. The trapezoidal element is an extension of the original two dimensional rectangular element, where $\theta \in [0, 1]$ is a relax parameter that

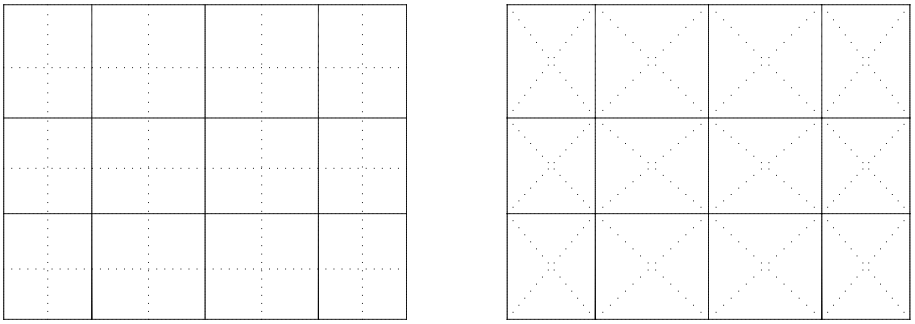

Fig. 1 *Left*: A rectangular mesh with nonoverlapping control volumes of interior vertices. *Right*: A rectangular mesh with overlapping control volumes of interior vertices

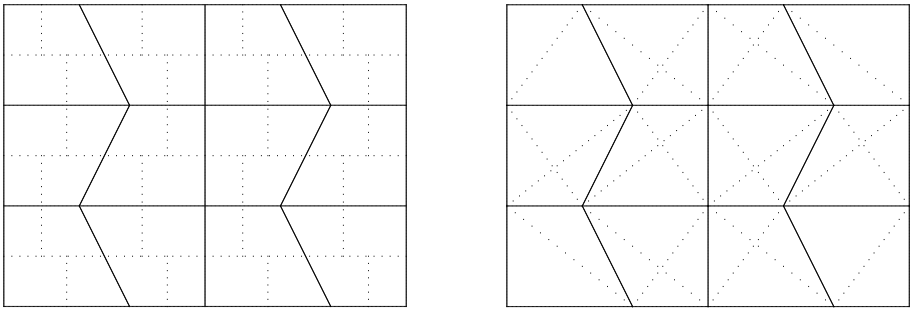

Fig. 2 *Left*: A trapezoid mesh with nonoverlapping control volumes. *Right*: A trapezoid mesh with overlapping control volumes

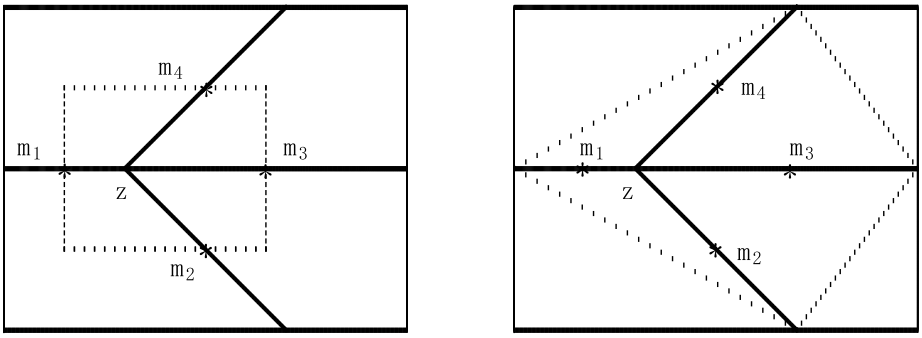

Fig. 3 *Left*: *(I)*. A sample nonoverlapping control volume V_z, where $m_i, i = 1, 2, 3, 4$, is midpoint. *Right*: *(II)*. A sample overlapping control volume V_z

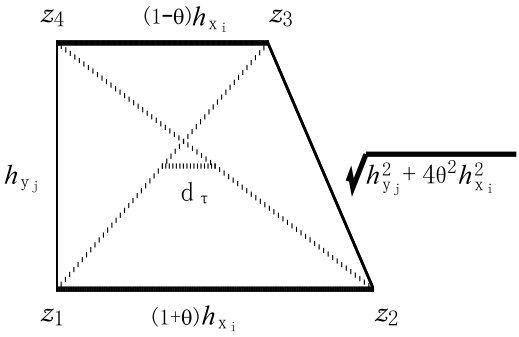

Fig. 4 The shape of a trapezoid element τ

depict the shape of a element, $z_i, i = 1, 2, 3, 4$, are vertexes of τ, and the length of the edge z_2z_3 equates $\sqrt{h_{y_j}^2 + 4\theta^2 h_{x_i}^2}$ in Fig. 4. When $\theta = 0$, the trapezoidal mesh degenerates to a rectangular mesh. When $\theta = 1$, the trapezoidal mesh degenerates to a triangle mesh.

Remark 2.2 For the low order conforming quadrilateral element, $Q_1(\tau) = span\{1, x, y, xy\}$. If we use Q_1-conforming element and the trapezoidal mesh in Fig. 2, then when $\theta = 1$, the trapezoid is degenerated into the right triangle. In this case, the Q_1-conforming quadrilateral

element is well-defined and it degenerates to the P_1-conforming triangular element [1, 13, 32]. For the P_1-nonconforming quadrilateral element, it has the same conclusion. Note that the smallness of the quantity d_τ, the distance between the two midpoints of the two diagonals of τ, is a good indicator of almost parallelogram [1, 11, 13, 20]. Here the midpoints distance $d_\tau = \theta h_{x_i}$ in Fig. 4. Obviously, $d_\tau \to 0$ as $\theta \to 0$, $Q_1(\tau)$ and $P_1(\tau)$ do work very well.

Now we introduce the standard notations and definitions for the Sobolev spaces $H^{m,p}(\Omega)$, and their associated norms $\|\cdot\|_{m,p}$ and seminorms $|\cdot|_{m,p}$, $m \geq 0$. If $p = 2$, the subscript p may be omitted, in which case the norms, inner products and seminorms are denoted by $\|\cdot\|_m$, $(\cdot,\cdot)_m$ and $|\cdot|_m$, respectively. If $m = 0$, the subscript m may be omitted. The space $H^0(\Omega)$ coincides with $L^2(\Omega)$, in which case the norm and inner product are denoted by $\|\cdot\|_0$ and $(\cdot,\cdot)$, respectively. The space $H_0^1(\Omega)$ is the subspace of $H^1(\Omega)$ consisting of functions with vanishing on $\partial\Omega$. Further we shall denote with p' the adjoint number of p, i.e. $\frac{1}{p} + \frac{1}{p'} = 1$, $p,\ p' \geq 1$. In what follows, we use C, with or without subscripts to denote a generic positive constant, possibly different at different occurrences in this paper, that is independent of the mesh parameter h but may depend on the domain Ω.

Let S_{0h} be the piecewise linear finite element space over the original partition T_h and $S_h^* \subset L^2(\Omega)$ be the piecewise constant space over the dual partition T_h^*, respectively. Suppose $z \in Z_h$ and denote the basis function of S_h at the vertex z by ϕ_z. Define V_z by the corresponding dual element of vertex z and χ_z by the characteristic function over V_z. Define the interpolation operator $I_h : H^2(\Omega) \cap H_0^1(\Omega) \to S_{0h}$ as in [34] such that

$$I_h\varphi(m) = \frac{1}{2}\big(\varphi(z_1) + \varphi(z_2)\big), \quad \forall m \in M_h,$$

where z_1 and z_2 are the endpoints of an edge with m as its midpoint. For any $\varphi \in H^2(\Omega) \cap H_0^1(\Omega)$, its interpolation can be expressed as

$$I_h\varphi = \frac{1}{2}\sum_{z\in Z_h} \varphi(z)\phi_z, \quad \forall \varphi \in H^2(\Omega) \cap H_0^1(\Omega). \tag{3}$$

It has the following approximation property

$$\|\varphi - I_h\varphi\| + h\|\varphi - I_h\varphi\|_{1,h} \leq Ch^2\|\varphi\|_2, \quad \forall \varphi \in H^2(\Omega) \cap H_0^1(\Omega).$$

Define a one-to-one operator $I_h^* : S_{0h} \to S_h^*$ by

$$I_h^*\varphi = \sum_{z\in Z_h} \varphi(z)\chi_z, \quad \forall \varphi \in S_{0h}. \tag{4}$$

It has the following approximation property [27]

$$\|\varphi - I_h^*\varphi\|_{0,q} \leq Ch|\varphi|_{1,q,h}, \quad \forall \varphi \in S_{0h},\ 1 < q < \infty.$$

In the finite volume discretization, we require the number of dual element should equal to the number of unknowns to obtain a unique approximate solution. For P_1-nonconforming quadrilateral element, the basis functions are corresponding to the vertices while continuous at the midpoints of the partition. So the standard finite volume scheme of problem (2) can read, finding $\overline{u}_h = \sum_{z_i \in Z_h^{in}} \overline{u}_{z_i}\phi_{z_i} \in S_{0h}$, such that

$$-\int_{\partial V_{z_i}} \frac{\partial \overline{u}_h}{\partial n} ds + \int_{V_{z_i}} f(\overline{u}_h)dxdy = \int_{V_{z_i}} g dxdy, \quad \forall z_i \in Z_h^{in}. \tag{5}$$

For convenience, we now define the finite volume scheme with interpolated coefficients, finding $u_h = \sum_{z_i \in Z_h^{in}} u_{z_i} \phi_{z_i} \in S_{0h}$, such that

$$-\int_{\partial V_{z_i}} \frac{\partial u_h}{\partial n} ds + \int_{V_{z_i}} J_h f(u_h) dxdy = \int_{V_{z_i}} g dxdy, \quad \forall z_i \in Z_h^{in}, \tag{6}$$

where $J_h f(u_h) = \sum_{z_i \in Z_h^{in}} f(u_{z_i}) \phi_{z_i}$.

Obviously, the nonlinear systems of FVM with interpolated coefficients (6) is simpler than that of the standard FVM (5) (or FEM) for the semilinear elliptic problems. If we use the Newton (or Newton-like) iteration method and P_1-nonconforming quadrilateral element to solve equations (6), it is easy to calculate its Jacobian matrix and stiffness matrix.

3 Preliminaries and Lemmas

Below we shall presume that the exact solution u of problem (1) is sufficiently smooth for our purpose. Next we introduce some bilinear forms and lemmas in this section. Defining

$$a\big(u, I_h^* \varphi_h\big) = -\sum_{z \in Z_h} \varphi_h(z) \int_{\partial V_z \setminus \partial T_h} \frac{\partial u}{\partial n} ds, \quad \forall \varphi_h \in S_{0h},$$

$$\big(u, I_h^* \varphi_h\big) = \sum_{z \in Z_h} \varphi_h(z) \int_{V_z} u dxdy, \quad \forall \varphi_h \in S_{0h},$$

and taking $V = V_z$, then problem (2) is rewritten as follows

$$a\big(u, I_h^* \varphi_h\big) + \big(f(u), I_h^* \varphi_h\big) = \big(g, I_h^* \varphi_h\big), \quad \forall \varphi_h \in S_{0h}. \tag{7}$$

Similarly, equation (6) is equivalent to finding $u_h \in S_{0h}$, such that

$$a\big(u_h, I_h^* \varphi_h\big) + \big(J_h f(u_h), I_h^* \varphi_h\big) = \big(g, I_h^* \varphi_h\big), \quad \forall \varphi_h \in S_{0h}. \tag{8}$$

Assume that T_h is a quasi-uniform trapezoid partition (see Fig. 2), the following two lemmas are suitable for the usual trapezoid mesh with rectangular control volumes. In terms of properties of interpolation and the bilinear form $a(\cdot, \cdot)$, we have

Lemma 3.1

$$a\big(\varphi_h, I_h^* \varphi_h\big) = |\varphi_h|_1^2, \qquad \forall \varphi_h \in S_{0h}, \tag{9}$$

$$a\big(u_h - I_h u, I_h^* \varphi_h\big) \le Ch \|u\|_2 |\varphi_h|_1, \quad \forall u \in H^2(\Omega) \cap H_0^1(\Omega),\ \varphi_h \in S_{0h}. \tag{10}$$

Proof For all $\varphi_h \in S_{0h}$, we can write it as follows

$$\varphi_h|_\tau = u_1 \phi_1 + u_2 \phi_2 + u_3 \phi_3 + u_4 \phi_4,$$

where u_k denotes the coefficient of the basis function ϕ_k, $k = 1, 2, 3, 4$. So we have

$$|\varphi_h|_1^2 = \sum_{\tau \in T_h} |\varphi_h|_{1,\tau}^2 = \sum_{\tau \in T_h} \int_\tau \left(\frac{\partial \varphi_h}{\partial x}\right)^2 dxdy + \int_\tau \left(\frac{\partial \varphi_h}{\partial y}\right)^2 dxdy = \sum_{\tau \in T_h} (\alpha_1 + \alpha_2),$$

where

$$\alpha_1 = \int_\tau \left(\frac{\partial \varphi_h}{\partial x}\right)^2 dxdy = \int_\tau \frac{1}{h_{x_i}^2}(u_2+u_3-u_1-u_4)^2 dxdy$$
$$= \frac{h_{y_j}}{h_{x_i}}(u_2+u_3-u_1-u_4)^2,$$
$$\alpha_2 = \int_\tau \left(\frac{\partial \varphi_h}{\partial y}\right)^2 dxdy = \int_\tau \frac{1}{h_{y_j}^2}(u_3+u_4-u_1-u_2)^2 dxdy$$
$$= \frac{h_{x_i}}{h_{y_j}}\big[u_3+u_4-u_1-u_2-\theta(u_1-u_2-u_3+u_4)\big]^2.$$

On the other hand, we have

$$a\big(\varphi_h, I_h^* \varphi_h\big) = -\sum_{z\in Z_h} \varphi_h(z) \int_{\partial V_z \setminus \partial T_h} \frac{\partial \varphi_h}{\partial n} ds$$
$$= -\sum_{\tau\in T_h} \sum_{i=1}^{4} \varphi_h(z_i) \int_{\partial V_{z_i}\cap\tau} \frac{\partial \varphi_h}{\partial n} ds$$
$$= -\sum_{\tau\in T_h} \big[\varphi_h(z_1)\beta_1 + \varphi_h(z_2)\beta_2 + \varphi_h(z_3)\beta_3 + \varphi_h(z_4)\beta_4\big],$$

where

$$\beta_1 = \int_{\partial V_{z_1}\cap\tau} \frac{\partial \varphi_h}{\partial n} ds = \frac{h_{y_j}}{2h_{x_i}}(u_2+u_3-u_1-u_4)$$
$$+ \frac{h_{x_i}}{2h_{y_j}}(1+\theta)\big[u_3+u_4-u_1-u_2+\theta(u_2+u_3-u_1-u_4)\big],$$
$$\beta_2 = \int_{\partial V_{z_2}\cap\tau} \frac{\partial \varphi_h}{\partial n} ds = \frac{h_{y_j}}{2h_{x_i}}(u_1+u_4-u_2-u_3)$$
$$+ \frac{h_{x_i}}{2h_{y_j}}(1-\theta)\big[u_3+u_4-u_1-u_2+\theta(u_2+u_3-u_1-u_4)\big],$$
$$\beta_3 = \int_{\partial V_{z_3}\cap\tau} \frac{\partial \varphi_h}{\partial n} ds = \frac{h_{y_j}}{2h_{x_i}}(u_1+u_4-u_2-u_3)$$
$$+ \frac{h_{x_i}}{2h_{y_j}}(1+\theta)\big[u_1+u_2-u_3-u_4+\theta(u_1+u_4-u_2-u_3)\big],$$
$$\beta_4 = \int_{\partial V_{z_4}\cap\tau} \frac{\partial \varphi_h}{\partial n} ds = \frac{h_{y_j}}{2h_{x_i}}(u_2+u_3-u_1-u_4)$$
$$+ \frac{h_{x_i}}{2h_{y_j}}(1-\theta)\big[u_1+u_2-u_3-u_4+\theta(u_1+u_4-u_2-u_3)\big]$$

and

$$\varphi_h(z_1) = \frac{1}{2}(3u_1 + u_2 - u_3 + u_4) + \frac{\theta}{2}(u_1 + u_4 - u_2 - u_3),$$
$$\varphi_h(z_2) = \frac{1}{2}(u_1 + 3u_2 + u_3 - u_4) + \frac{\theta}{2}(u_2 + u_3 - u_1 - u_4),$$
$$\varphi_h(z_3) = \frac{1}{2}(-u_1 + u_2 + 3u_3 + u_4) + \frac{\theta}{2}(u_1 + u_4 - u_2 - u_3),$$
$$\varphi_h(z_4) = \frac{1}{2}(u_1 - u_2 + u_3 + 3u_4) + \frac{\theta}{2}(u_2 + u_3 - u_1 - u_4).$$

From above equalities, we obtain

$$\begin{aligned}\alpha_1 + \alpha_2 &= -\big[\varphi_h(z_1)\beta_1 + \varphi_h(z_2)\beta_2 + \varphi_h(z_3)\beta_3 + \varphi_h(z_4)\beta_4\big] \\ &= \frac{h_{y_j}}{h_{x_i}}(u_2 + u_3 - u_1 - u_4)^2 + \frac{h_{x_i}}{h_{y_j}}\big[u_3 + u_4 - u_1 - u_2 - \theta(u_1 - u_2 - u_3 + u_4)\big]^2.\end{aligned}$$

The desired result (9) is derived from above formulations. From [27, 36] we also have (10). □

Remark 3.1 From [36, 41], the following result is classical for the semilinear elliptic equation (1) by using Q_1-conforming rectangular element, i.e.,

$$a\big(\varphi_h, \widetilde{I}_h^*\varphi_h\big) \geq \frac{1}{2}|\varphi_h|_1^2, \quad \forall \varphi_h \in \widetilde{S}_{0h},$$

where $\widetilde{S}_{0h}$ is the piecewise bilinear finite element space over the rectangular partition and $\widetilde{I}_h^* : C(\Omega) \to S_h^*$ is the interpolation operator correspondingly. From equation (9), we know that $a(\cdot,\cdot)$ has better coercivity and stability for P_1-nonconforming rectangular element.

Remark 3.2 In fact, for the general quadrilateral mesh with two types of control volumes in Fig. 3, if we use P_1-nonconforming quadrilateral FVM to solve the semilinear elliptic equation (1), then we can obtain the same properties of bilinear form $a(\cdot,\cdot)$ by the symbolic computation and the similar technique in [27, 36], i.e., (9) and (10) hold.

Form [16, 27], we have following useful lemma.

Lemma 3.2 *The semi-norm $|\cdot|_1$ and the norm $\|\cdot\|_1$ are equivalent in the space S_{0h}, that is, there exists positive constants C_1 and C_2, such that*

$$C_1|\varphi_h|_1 \leq \|\varphi_h\|_1 \leq C_2|\varphi_h|_1, \quad \forall \varphi_h \in S_{0h}.$$

Lemma 3.3 *For the quasi-uniform rectangular mesh, the operator I_h^* has following properties*

$$\int_\tau I_h^* v_h dxdy = \int_\tau v_h dxdy, \qquad \forall v_h \in S_{0h},\ \forall \tau \in T_h, \tag{11}$$

$$\int_{z_k z_{k+1}} I_h^* v_h ds = \int_{z_k z_{k+1}} v_h ds, \qquad \forall v_h \in S_{0h},\ \forall \tau \in T_h, \tag{12}$$

$$\|v_h - I_h^* v_h\|_{0,p,\tau} \le Ch|v_h|_{1,p,\tau}, \quad \forall v_h \in S_{0h},\ \forall \tau \in T_h,\ 1 < p < \infty. \tag{13}$$

Proof Consider $\tau \in T_h$ (as in Fig. 4), where $z_5 = z_1$ and $\theta = 0$. For all $v_h \in S_{0h}$, we have

$$v_h|_\tau = u_1\phi_1 + u_2\phi_2 + u_3\phi_3 + u_4\phi_4$$

and

$$\begin{aligned}
\int_\tau I_h^* v_h dxdy &= \frac{h_{x_i}h_{y_j}}{4}\big[v_h(z_1) + v_h(z_2) + v_h(z_3) + v_h(z_4)\big] \\
&= \frac{h_{x_i}h_{y_j}}{4}(2u_1 + 2u_2 + 2u_3 + 2u_4) \\
&= \frac{h_{x_i}h_{y_j}}{2}(u_1 + u_2 + u_3 + u_4), \\
\int_\tau v_h dxdy &= \int_\tau (u_1\phi_1 + u_2\phi_2 + u_3\phi_3 + u_4\phi_4)dxdy \\
&= \frac{h_{x_i}h_{y_j}}{2}(u_1 + u_2 + u_3 + u_4).
\end{aligned}$$

The equation (11) is derived from above two equalities.

On one hand, for $k = 1$ and $k = 3$, we have

$$\begin{aligned}
&\int_{z_k z_{k+1}} v_h ds = \int_{z_k z_{k+1}} (u_1\phi_1 + u_2\phi_2 + u_3\phi_3 + u_4\phi_4)ds = (u_k + u_{k+1})h_{x_i}, \\
&\int_{z_k z_{k+1}} I_h^* v_h ds = \frac{h_{x_i}}{2}\big[v_h(z_k) + v_h(z_{k+1})\big] = \frac{h_{x_i}}{2}(2u_k + 2u_{k+1}) = (u_k + u_{k+1})h_{x_i}.
\end{aligned}$$

On the other hand, for $k = 2$ and $k = 4$, we have

$$\begin{aligned}
&\int_{z_k z_{k+1}} v_h ds = \int_{z_k z_{k+1}} (u_1\phi_1 + u_2\phi_2 + u_3\phi_3 + u_4\phi_4)ds = (u_k + u_{k+1})h_{y_j}, \\
&\int_{z_k z_{k+1}} I_h^* v_h ds = \frac{h_{y_j}}{2}\big[v_h(z_k) + v_h(z_{k+1})\big] = \frac{h_{y_j}}{2}(2u_k + 2u_{k+1}) = (u_k + u_{k+1})h_{y_j},
\end{aligned}$$

where $u_5 = u_1$. Equation (12) is derived from above four equalities. □

Apply the similar technique in [7, 27], we also obtain inequality (13).

Remark 3.3 If we use the trapezoidal mesh with rectangular control volumes to instead of rectangular mesh in Fig. 2, equation (11) can rewrite as

$$\left|\int_\tau I_h^* v_h dxdy - \int_\tau v_h dxdy\right| \le Ch^2\|v_h\|_{1,\tau}, \quad \forall v_h \in S_{0h}, \tau \in T_h. \tag{14}$$

For all $\tau \in T_h$ as in Fig. 4, we have

$$v_h|_\tau = u_1\phi_1 + u_2\phi_2 + u_3\phi_3 + u_4\phi_4.$$

By simple computation, we obtain

$$\begin{aligned}\int_\tau I_h^* v_h dxdy &= \frac{h_{x_i}h_{y_j}}{4}\big[v_h(z_1)(1+\theta)+v_h(z_2)+v_h(z_3)+v_h(z_4)(1-\theta)\big]\\ &= \frac{h_{x_i}h_{y_j}}{4}\big[\big(2+\theta+\theta^2\big)u_1+\big(2+\theta-\theta^2\big)u_2+\big(2-\theta-\theta^2\big)u_3\\ &\quad+\big(2-\theta+\theta^2\big)u_4\big].\\ \int_\tau v_h dxdy &= \int_\tau (u_1\phi_1+u_2\phi_2+u_3\phi_3+u_4\phi_4)dxdy\\ &= h_{x_i}h_{y_j}\left[\frac{3+\theta}{6}(u_1+u_2)+\frac{3-\theta}{6}(u_3+u_4)\right].\end{aligned}$$

By combining of these results, we obtain

$$\begin{aligned}&\left|\int_\tau I_h^* v_h dxdy-\int_\tau v_h dxdy\right|\\ &= \frac{h_{x_i}h_{y_j}}{4}\left|\theta^2(u_1+u_4-u_2-u_3)+\frac{\theta}{3}(u_1+u_2-u_3-u_4)\right|\\ &= \frac{h_{x_i}h_{y_j}}{4}\left|\frac{2\theta^2}{3}(u_1+u_4-u_2-u_3)+\frac{\theta}{3}\big[(1+\theta)(u_1-u_3)+(1-\theta)(u_2-u_4)\big]\right|\\ &\le \frac{h^2}{4}\left\{\frac{8\theta^4}{9}(u_1+u_4-u_2-u_3)^2+\frac{2\theta^2}{9}\big[(1+\theta)(u_1-u_3)+(1-\theta)(u_2-u_4)\big]^2\right\}^{\frac{1}{2}}\\ &\le Ch^2\big\{(u_1+u_4-u_2-u_3)^2+\big[(1+\theta)(u_1-u_3)+(1-\theta)(u_2-u_4)\big]^2\big\}^{\frac{1}{2}}\\ &= Ch^2|v_h|_{1,\tau}\le Ch^2\|v_h\|_{1,\tau}.\end{aligned}$$

By symbolic computation, we have the same result (12) for the trapezoidal mesh with rectangular control volumes. Here

$$\begin{aligned}\int_{z_1z_2} v_h ds &= \int_{z_1z_2}(u_1\phi_1+u_2\phi_2+u_3\phi_3+u_4\phi_4)ds=(u_1+u_2)(1+\theta)h_{x_i},\\ \int_{z_1z_2} I_h^* v_h ds &= \frac{(1+\theta)h_{x_i}}{2}\big[v_h(z_1)+v_h(z_2)\big]=\frac{(1+\theta)h_{x_i}}{2}(2u_1+2u_2)=\int_{z_1z_2} v_h ds,\\ \int_{z_2z_3} v_h ds &= \int_{z_2z_3}(u_1\phi_1+u_2\phi_2+u_3\phi_3+u_4\phi_4)ds\\ &= (u_2+u_3)\sqrt{h_{y_j}^2+4\theta^2h_{x_i}^2},\\ \int_{z_2z_3} I_h^* v_h ds &= \frac{\sqrt{h_{y_j}^2+4\theta^2h_{x_i}^2}}{2}\big[v_h(z_2)+v_h(z_3)\big]=\frac{\sqrt{h_{y_j}^2+4\theta^2h_{x_i}^2}}{2}(2u_2+2u_3)\\ &= \int_{z_2z_3} v_h ds,\end{aligned}$$

$$\int_{z_3z_4} v_h ds = \int_{z_3z_4} (u_1\phi_1 + u_2\phi_2 + u_3\phi_3 + u_4\phi_4) ds = (u_3 + u_4)(1-\theta)h_{x_i},$$

$$\int_{z_3z_4} I_h^* v_h ds = \frac{(1-\theta)h_{x_i}}{2}\big[v_h(z_3) + v_h(z_4)\big] = \frac{(1-\theta)h_{x_i}}{2}(2u_3 + 2u_4) = \int_{z_3z_4} v_h ds,$$

$$\int_{z_4z_1} v_h ds = \int_{z_4z_1} (u_1\phi_1 + u_2\phi_2 + u_3\phi_3 + u_4\phi_4) ds = (u_4 + u_1)h_{y_j},$$

$$\int_{z_4z_1} I_h^* v_h ds = \frac{h_{y_j}}{2}\big[v_h(z_4) + v_h(z_1)\big] = \frac{h_{y_j}}{2}(2u_4 + 2u_1) = \int_{z_4z_1} v_h ds.$$

Moreover, we use inequality (14) and apply the similar technique in [7, 27], and also obtain inequality (13) for the trapezoidal mesh with rectangular control volumes.

It is pointed out that we can obtain the similar results (12), (13) and (14) by using symbolic computation on the general quadrilateral mesh for P_1-nonconforming quadrilateral FVM with two types of control volumes.

By using the similar technique in [7, 27], we also have the following result.

Lemma 3.4 *Assume v, w are sufficiently smooth functions. Let $I_h w \in S_{0h}$ be the interpolation of w, then*

$$\big|\big(v \cdot (w - I_h w), \varphi_h\big)\big| \le Ch^2 \|w\|_{2,p} \|\varphi_h\|_{1,p'}, \quad \forall \varphi_h \in S_{0h} \tag{15}$$

for $\frac{1}{p} + \frac{1}{p'} = 1, 1 < p \le \infty$.

Lemma 3.5 *Assume $w \in H^2(\Omega) \bigcap H_0^1(\Omega)$, then there exists a positive constant C independent of the mesh size h, such that*

$$\big|\big(w - I_h w, I_h^* \varphi_h\big)\big| \le Ch^2 \|w\|_2 \|\varphi_h\|_1, \quad \forall \varphi_h \in S_{0h}. \tag{16}$$

Proof Using Lemma 3.4 and the Schwartz inequality, we obtain

$$\begin{aligned}\big|\big(w - I_h w, \varphi_h - I_h^* \varphi_h\big)\big| &\le \sum_{\tau \in T_h} \int_\tau |w - I_h w||\varphi_h - I_h^* \varphi_h| dx dy \\ &\le \sum_{\tau \in T_h} C_\tau h^3 \|w\|_{2,\tau} \|\varphi_h\|_{1,\tau} \le Ch^3 \|w\|_2 \|\varphi_h\|_1. \end{aligned} \tag{17}$$

By using (17) and (15) with $v \equiv 1$ and $p = 2$, we get the desired result (16). □

4 Error Estimates

In this section, we provide some error estimates for the finite volume scheme (6). Firstly we introduce an auxiliary bilinear form

$$A\big(u; w, I_h^* \varphi_h\big) = a\big(w, I_h^* \varphi_h\big) + \big(f'(u)w, I_h^* \varphi_h\big),$$

where u is the exact solution of problem (2). For the auxiliary bilinear form $A(u; \cdot, \cdot)$, we have following positive definite properties.

Lemma 4.1 *For $u \in H_0^1(\Omega)$, $A(u; w_h, I_h^* w_h)$ is positive definite for sufficiently small h, i.e., there exists a positive constant γ, such that*

$$A\big(u; w_h, I_h^* w_h\big) \geq \gamma(u, f)\|w_h\|_1^2. \tag{18}$$

Proof We rewrite $A(u; w_h, I_h^* w_h)$ as follows

$$A\big(u; w_h, I_h^* w_h\big) = a\big(w_h, I_h^* w_h\big) + \big(f'(u)w_h, w_h\big) - \big(f'(u)w_h, w_h - I_h^* w_h\big). \tag{19}$$

From Lemmas 3.1 and 3.2, we have

$$a\big(w_h, I_h^* w_h\big) \geq C_1\|w_h\|_1^2. \tag{20}$$

Note that $f'(s) > 0$ and let $C_2 = \inf_{z\in\Omega} f'(u(z))$, then we have

$$\big(f'(u)w_h, w_h\big) \geq C_2\|w_h\|_0^2 \geq 0. \tag{21}$$

In terms of (11) in Lemma 3.3, Remarks 3.1 and 3.2, we obtain

$$\begin{aligned}
\big|\big(f'(u)w_h, w_h - I_h^* w_h\big)\big| &= \Big|\sum_{\tau\in T_h}\int_\tau f'(u)w_h\big(w_h - I_h^* w_h\big)dxdy\Big| \\
&\leq \sum_{\tau\in T_h}\Big[\Big|\int_\tau \big(f'(u)w_h - C_\tau\big)\big(w_h - I_h^* w_h\big)dxdy\Big| + Ch^2\|w_h\|_{1,\tau}^2\Big] \\
&\leq \sum_{\tau\in T_h}\big[C_3 h|f'(u)w_h|_{1,\tau}h|w_h|_{1,\tau} + Ch^2\|w_h\|_{1,\tau}^2\big] \\
&\leq \max_\Omega\big(|f''(u)\nabla u|, |f'(u)|\big)\sum_{\tau\in T_h} C_4 h^2\|w_h\|_{1,\tau}^2 + Ch^2\|w_h\|_1^2 \\
&\leq C_5 h^2\|w_h\|_1^2,
\end{aligned} \tag{22}$$

where C_τ is the value of $f'(u)w_h$ at the center point in $\tau \in T_h$. Using (20), (21) and (22), we obtain

$$A\big(u; w_h, I_h^* w_h\big) \geq C_1\|w_h\|_1^2 - C_5 h^2\|w_h\|_1^2 = \big(C_1 - C_5 h^2\big)\|w_h\|_1^2,$$

which implies the desired result (18) for sufficiently small h. □

Next we derive the main result of this section.

Theorem 4.1 *Assume $u \in \mathrm{H}^2(\Omega)\bigcap \mathrm{H}_0^1(\Omega)$ is the solution of problem (1) and T_h is quasi-uniform rectangular or trapezoidal partition of domain Ω, then the approximate solution $u_h \in S_{0h}$ of FVM with interpolated coefficients (6) converges to the exact solution u and has the following estimate*

$$\|u - u_h\|_1 \leq C(u, f)h \tag{23}$$

for sufficiently small h.

Proof Subtracting (8) from (7), we obtain the following error equation

$$a\big(u-u_h, I_h^*\varphi_h\big)+\big(f(u)-J_hf(u_h), I_h^*\varphi_h\big)=0. \tag{24}$$

Define

$$f(u)-J_hf(u_h)=\big(f(u)-J_hf(u)\big)+J_h\big(f(u)-f(u_h)\big)=\lambda_1+\lambda_2, \tag{25}$$

where $\lambda_1=f(u)-J_hf(u)$. Next we analyze the function $f(u)-J_hf(u_h)$. By using Taylor expansion in $\tau\in T_h$, we have

$$\begin{aligned}\lambda_2&=J_h\big(f(u)-f(u_h)\big)=\sum_{z\in Z_h(\tau)}\big(f\big(u(z)\big)-f\big(u_h(z)\big)\big)\phi_z\\&\le f'(u)(I_hu-u_h)+\delta_1\max_{\tau}|I_hu-u_h|+\delta_2\max_{\tau}|I_hu-u_h|^2\\&=f'(u)(I_hu-u_h)+\lambda_3,\end{aligned} \tag{26}$$

where

$$\begin{aligned}\lambda_3&=\delta_1\max_{\tau}|I_hu-u_h|+\delta_2\max_{\tau}|I_hu-u_h|^2,\\\delta_1&=C\max_{z',z''\in\tau}|f'(u(z'))-f'(u(z''))|=o(h),\\\delta_2&=\frac{1}{2}f''(\xi)=o(1).\end{aligned}$$

Substituting (26) into (24), we have

$$A\big(u;u_h-I_hu, I_h^*\varphi_h\big)=a\big(u-I_hu, I_h^*\varphi_h\big)+\big(\lambda_1+\lambda_3, I_h^*\varphi_h\big).$$

Letting $\zeta=u_h-I_hu\in S_{0h}$ and taking $\varphi_h=\zeta$, from Lemmas 3.5 and 4.1, we obtain

$$\gamma\|\zeta\|_1^2\le Ch\|\zeta\|_1+C\big(h\|\zeta\|_{0,\infty}+\|\zeta\|_{0,\infty}^2\big)\|\zeta\|_{0,1}.$$

Recalling for Bramble [3], that

$$\|\zeta\|_{0,\infty}\le C|\ln h|^{1/2}\|\nabla\zeta\|\le C|\ln h|^{1/2}\|\zeta\|_1$$

hold for all $\zeta\in S_{0h}$ and using the well know Sobolev inequality

$$\|v\|_{0,p}\le C\|v\|_1,\quad \forall 1\le p<\infty,$$

we get

$$\gamma\|\zeta\|_1^2\le Ch\|\zeta\|_1+C\big(h|\ln h|^{1/2}\|\zeta\|_1+|\ln h|\|\zeta\|_1^2\big)\|\zeta\|_1.$$

Omitting the common factor $\|\zeta\|_1$, we have

$$\gamma\|\zeta\|_1\le Ch+Ch|\ln h|^{1/2}\|\zeta\|_1+C|\ln h|\|\zeta\|_1^2 \tag{27}$$

for sufficiently small h.

Omitting the second term of the right-side of (27), we get

$$\|\zeta\|_1 \le C_1 h + C_2 |\ln h| \|\zeta\|_1^2. \tag{28}$$

Next we adopt a continuity argument by imitating the method in [17] and prove

$$\|\zeta\|_1 \le \|I_h u - u_h\| \le 2C_1 h. \tag{29}$$

For all $b \in [0, 1]$, considering the following auxiliary semilinear elliptic problems (P^b): Find u^b such that

$$\begin{cases} -\Delta u^b + bf(u^b) = bg & \text{in } \Omega, \\ u^b = 0 & \text{on } \partial\Omega. \end{cases} \tag{30}$$

Obviously, when $b = 1$, this is the original problem (1). And when $b = 0$, we have the exact solution $u^0 = 0$. We shall assume the following condition on $\Omega = (0, 1) \times (0, 1)$. $\forall b \in [0, 1]$, there exist a solution u^b of problem (P^b) and a positive constant ξ, such that the set

$$N_\xi = \left\{ \omega | \omega \in H^2(\Omega) \bigcap H_0^1(\Omega), \max_{\Omega} |u - \omega| < \xi \right\}$$

is some neighborhood of the exact solution u of problem (1).

We approximate the problem (P^b): Find $u_h^b \in S_{0h}$, such that

$$a\big(u_h^b, I_h^* v_h\big) + b\big(J_h f\big(u_h^b\big), I_h^* v_h\big) = b\big(g, I_h^* v_h\big), \quad \forall v_h \in S_{0h}. \tag{31}$$

We intend to show that (P_h^b) is solvable. For each h, we define the set $F_h \subset [0, 1]$ by

$$F_h = \big\{ b \in [0, 1] | \big(P_h^b\big) \text{ has a solution } u_h^b \in N_\xi \text{ and } \|I_h u^b - u_h^b\|_1 \le 2C_1 h \text{ holds} \big\},$$

where C_1 is the constant appearing in (28). Next we show that the set F_h has the following properties.

(i) F_h is not empty. In fact, for $b = 0$, $u^b = 0$ and $u_h^b = 0$ are the solutions of continuous and the discrete problems, respectively.

(ii) F_h is open in [0, 1]. If $b \in F_h$, then (P_h^b) is solvable. Using the monotonicity condition, we obtain the solvability of (P_h^b) for all points $\widetilde{b}$ in a neighborhood of b. By the implicit function theorem, $u_h^{\widetilde{b}}$ depends continuously on $\widetilde{b}$. Thus properly shorten the neighborhood such that the strict inequality $\|I_h u^b - u_h^b\|_1 \le 2C_1 h$ and $u_h^b \in N_\xi$ is still valid and we have $\widetilde{b} \in F_h$ for these $\widetilde{b}$.

(iii) F_h is closed. Let $b(j) \in F_h$ and $b(j) \to b$, $j \to \infty$. Since $u_h^{b(j)} \in N_\xi$, there is a cluster point u_h^b which is the unique solution of (P_h^b) and satisfies $\|I_h u^b - u_h^b\|_1 \le 2C_1 h$. Recalling for (28), we conclude

$$\|I_h u^b - u_h^b\|_1 \le C_1 h + 4C_2 C_1^2 |\ln h| h^2 \le C_1 (1 + 4C_1 C_2 |\ln h| h) h.$$

Then for sufficiently small h, we have $4C_1 C_2 |\ln h| h \le 1$ and $\|I_h u^b - u_h^b\|_1 \le 2C_1 h$, i.e., the strict inequality holds.

Form (i)–(iii), we know that for sufficiently small h, the set F_h is not empty, closed and open with respect to b and thus must coincide with [0,1]. Note that for $b = 1$, (P_h^1) is solvable. We prove that (29) and $u_h \in N_\xi$ hold for appropriately small h.

Finally, the desired result (23) follows form (29) and the approximation property

$$\|u - I_h u\|_1 \le Ch \|u\|_2. \qquad \square$$

5 Superconvergence of Derivative

In this section we show superconvergence of derivative of the finite volume scheme (6) on the rectangular mesh. First we give the superclose property of derivative for $I_h u$.

Lemma 5.1 [20, 25] *For sufficiently smooth function u, let $I_h u \in S_{0h}$ be the interpolation of u on the rectangular mesh, then we have superclose property*

$$|\nabla(u - I_h u)| = o\big(h^2 |\ln h|\big) \tag{32}$$

for the center points in all $\tau \in T_h$.

For the FVM with interpolated coefficients (6) on the rectangular mesh for the semilinear elliptic problem, we have the following superconvergence results of derivative.

Theorem 5.1 *Assume that $u \in W_\infty^3(\Omega)$, $f'(s) > 0$ for $s \in (-\infty, +\infty)$ and $f''(s)$ is continuous with respect to s, and $g \in W_0^1(\Omega)$. Assume that the rectangular partition T_h of Ω is the quasi uniform. Then the FVM with interpolated coefficients (6) for the semilinear elliptic problem has superconvergence of derivative, i.e.,*

$$|\nabla(u - u_h)| = o\big(h^2 |\ln h|\big)$$

hold for all center points of $\tau \in T_h$.

Proof Choosing $v = v_h \in S_{0h}$ in (7), we obtain

$$a(u, v_h) + \big(f(u), v_h\big) = (g, v_h). \tag{33}$$

Subtracting (8) from (33), we have

$$\begin{aligned} &a(u - u_h, v_h) + a\big(u, v_h - I_h^* v_h\big) + a\big(u_h - u, v_h - I_h^* v_h\big) + \big(f(u) - J_h f(u), v_h\big) \\ &\quad + \big(J_h f(u), v_h - I_h^* v_h\big) + \big(J_h\big(f(u) - f(u_h)\big), I_h^* v_h\big) = (g, v_h) - \big(g, I_h^* v_h\big). \end{aligned} \tag{34}$$

Let $\eta = u - I_h u$, $\zeta = u_h - I_h u$. It follows from (34), (25) and (26) that

$$\begin{aligned} A(u; \zeta, v_h) &= a(\zeta, v_h) + \big(f'(u)\zeta, v_h\big) \\ &= a(\eta, v_h) + a\big(u, v_h - I_h^* v_h\big) + a\big(u_h - u, v_h - I_h^* v_h\big) + (\lambda_1, v_h) \\ &\quad + \big(J_h f(u), v_h - I_h^* v_h\big) + \big(\lambda_3, I_h^* v_h\big) + \big(g, I_h^* v_h - v_h\big). \end{aligned} \tag{35}$$

Recalling [7], we get

$$|a(\eta, v_h)| = \left| \int_\Omega \nabla\eta \nabla v_h dx dy \right| \le Ch^2 \|u\|_{3,\infty} \|v_h\|_{1,1}. \tag{36}$$

Using Lemma 3.4 with $p = +\infty$, we have

$$|(\lambda_1, v_h)| = |\big(f(u) - J_h f(u), v_h\big)| \le Ch^2 \|f(u)\|_{2,\infty} \|v_h\|_{1,1}. \tag{37}$$

In terms of Lemma 3.3 and the trace theorem, we have

$$\begin{aligned}\left|a\left(u, v_h - I_h^* v_h\right)\right| &= \left|\sum_{V\in T_h^*}\left(\int_V \nabla u \nabla v_h dx dy - v_h(z)\int_{\partial V}\frac{\partial u}{\partial n} ds\right)\right| \\ &= \left|\sum_{V\in T_h^*}\int_{\partial V}\frac{\partial u}{\partial n}\left(v_h - v_h(z)\right) ds\right| \\ &= \left|\sum_{\tau\in T_h}\sum_{i=1}^{4}\int_{\partial V_{z_i}\cap\tau}\left(\frac{\partial u}{\partial n} - w_\tau\right)\left(v_h - I_h^* v_h\right) ds\right| \\ &\le Ch^2\|u\|_{2,\infty}\|v_h\|_{1,1}, \end{aligned} \tag{38}$$

where w_τ is the value of $\frac{\partial u}{\partial n}$ at the midpoint on the edge $z_i z_{i+1}$, $i = 1, 2, 3, 4$, and $z_5 = z_1$. Analogously, we get

$$\begin{aligned}\left|a\left(u_h - u, v_h - I_h^* v_h\right)\right| &= \left|\sum_{\tau\in T_h}\sum_{i=1}^{4}\int_{z_i z_{i+1}}\frac{\partial(u_h - u)}{\partial n}\left(v_h - I_h^* v_h\right) ds\right| \\ &\le Ch\|u_h - u\|_{1,\infty}\|v_h\|_{0,1} \\ &\le Ch\|u_h - u\|_{1,\infty}\|v_h\|_{1,1}. \end{aligned} \tag{39}$$

Using Lemma 3.3, we obtain the following estimates

$$\left|\left(J_h f(u), v_h - I_h^* v_h\right)\right| \le Ch^2\|f(u)\|_{1,\infty}\|v_h\|_{1,1}, \tag{40}$$

$$\left|\left(g, v_h - I_h^* v_h\right)\right| \le Ch^2\|g\|_{1,\infty}\|v_h\|_{1,1}. \tag{41}$$

Substituting from (36)–(41) into (35), we have

$$A(u;\zeta, v_h) \le Ch^2\|v_h\|_{1,1} + Ch\|u_h - u\|_{0,\infty}\|v_h\|_{1,1} + C\|\lambda_3\|_{0,\infty}\|v_h\|_{1,1}.$$

Note that

$$\|u_h - u\|_{0,\infty} \le \|\eta\|_{0,\infty} + \|\zeta\|_{0,\infty} \le C(u)h^2 + \|\zeta\|_{0,\infty}$$

and

$$\|\lambda_2\|_{0,\infty} \le Ch\|\zeta\|_{0,\infty} + Ch\|\zeta\|_{0,\infty}^2,$$

this yields

$$A(u;\zeta, v_h) \le Ch^2\|v_h\|_{1,1} + Ch\|\zeta\|_{1,\infty}\|v_h\|_{1,1} + C\|\zeta\|_{1,\infty}\|v_h\|_{1,1}. \tag{42}$$

Choosing $v_h = G_h$ as the discrete Green function with respect to the bilinear form $A(u_h;\cdot,\cdot)$, and noting that $\|G_h\|_{1,1} \le |\ln h|$ (see [7]), we get

$$\|\zeta\|_{1,\infty} \le Ch^2|\ln h| + Ch\|\zeta\|_{1,\infty}|\ln h| + C\|\zeta\|_{1,\infty}^2|\ln h|.$$

For sufficiently small h, omitting the second term of the right-side, we have

$$\|\zeta\|_{1,\infty} \le Ch^2|\ln h| + C\|\zeta\|_{1,\infty}^2|\ln h|. \tag{43}$$

Similarly, we adopt the continuity argument in the proof of Theorem 4.1 and obtain

$$|\nabla\zeta|_{0,\infty} \le \|\zeta\|_{1,\infty} \le Ch^2|\ln h|. \tag{44}$$

Using (32) and (44), we obtain

$$|\nabla(u-u_h)| \le |\nabla(u-I_hu)| + |\nabla\zeta| = |\nabla(u-I_hu)| + o\big(h^2|\ln h|\big),$$

i.e.,

$$|\nabla(u-u_h)| = o\big(h^2|\ln h|\big),$$

for all the center points of $\tau \in T_h$. This completes the proof of the theorem. □

Remark 5.1 For Q_1-conforming rectangular element, if $I_hu \in \widetilde{S}_{0h}$ is the Lagrange interpolation of u, then the following superclose property [40]

$$|\nabla(u-I_hu)| = o\big(h^2\big)$$

holds for the center points for all $\tau \in T_h$. Moreover, the similar superconvergence result of derivative in Theorem 5.1 also holds.

6 Numerical Experiments

In this section, we present one test problem to illustrate the theoretical results obtained in the previous section. In our numerical experiments, we consider the following semilinear elliptic problem on a unit square domain Ω in R^2:

$$-\Delta u + u^3 = g, \quad \text{in } \Omega, \qquad u = 0, \quad \text{on } \partial\Omega \tag{45}$$

where the exact solution is given by

$$u(x,y) = y(1-x)\sin\big(x(1-y)\big),$$

and the right-hand side function g is generated by problem (45). Here we use the nonuniform triangulations of Ω into quadrilaterals [16]. The quadrilateral meshes are depicted in Fig. 5. Each element is a right trapezoid whose the shape is controlled by a relax parameter $\theta \in [0,1]$, see Fig. 6. Here, for any fixed θ, the meshes do not satisfy the nearly parallelogram condition when h decreases. When $\theta = 0$, each element is a rectangle. When $\theta = 1$, each element is a right triangle.

Firstly, we apply P_1-nonconforming quadrilateral FVM to the test problem (45) based on nonoverlapping control volume (I) and overlapping control volume (II) in Fig. 3, respectively. And then we use P_1-nonconforming quadrilateral FEM to the test problem (45). Numerical results on the trapezoidal meshes are presented in Tables 1, 2 and 3 in terms of the H^1-seminorm convergence rates. Here we only present five cases for $\theta = 0, \frac{1}{4}, \frac{1}{2}, \frac{3}{4}$ and 1. From these tables, we observe that the convergence rates are optimal on these general quadrilateral meshes, which confirms well our theoretical analysis. But the relatively errors $\frac{|u-u_h|}{|u|}$ of three methods by using P_1-nonconforming quadrilateral element increase as θ increases, respectively.

Table 1 FVM with P_1-nonconforming quadrilateral element based on nonoverlapping control volume

N	$\theta=0$		$\theta=\frac{1}{4}$		$\theta=\frac{1}{2}$		$\theta=\frac{3}{4}$		$\theta=1$	
	$\frac{\lvert u-u_h\rvert}{\lvert u\rvert}$	Rate	$\frac{\lvert u-u_h\rvert}{\lvert u\rvert}$	Rate	$\frac{\lvert u-u_h\rvert}{\lvert u\rvert}$	Rate	$\frac{\lvert u-u_h\rvert}{\lvert u\rvert}$	Rate	$\frac{\lvert u-u_h\rvert}{\lvert u\rvert}$	Rate
4	2.3883e-1	–	2.4899e-1	–	2.7641e-1	–	3.1922e-1	–	3.7512e-1	–
8	1.1924e-1	1.0032	1.2495e-1	0.9947	1.4099e-1	0.9713	1.6606e-1	0.9428	1.9891e-1	0.9153
16	5.9588e-2	1.0007	6.2512e-2	0.9992	7.0766e-2	0.9945	8.3675e-2	0.9889	1.0059e-1	0.9835
32	2.9790e-2	1.0002	3.1259e-2	0.9999	3.5412e-2	0.9988	4.1907e-2	0.9976	5.0420e-2	0.9965
64	1.4895e-2	1.0000	1.5629e-2	1.0000	1.7709e-2	0.9998	2.0961e-2	0.9995	2.5224e-2	0.9992

Table 2 FVM with P_1-nonconforming quadrilateral element based on overlapping control volume

N	$\theta=0$		$\theta=\frac{1}{4}$		$\theta=\frac{1}{2}$		$\theta=\frac{3}{4}$		$\theta=1$	
	$\frac{\lvert u-u_h\rvert}{\lvert u\rvert}$	Rate	$\frac{\lvert u-u_h\rvert}{\lvert u\rvert}$	Rate	$\frac{\lvert u-u_h\rvert}{\lvert u\rvert}$	Rate	$\frac{\lvert u-u_h\rvert}{\lvert u\rvert}$	Rate	$\frac{\lvert u-u_h\rvert}{\lvert u\rvert}$	Rate
4	2.3508e-1	–	2.4722e-1	–	2.7963e-1	–	3.2832e-1	–	3.8870e-1	–
8	1.1876e-1	0.9851	1.2535e-1	0.9797	1.4354e-1	0.9620	1.7100e-1	0.9411	2.0529e-1	0.9210
16	5.9527e-2	0.9964	6.2882e-2	0.9952	7.2194e-2	0.9915	8.6229e-2	0.9877	1.0374e-1	0.9847
32	2.9782e-2	0.9991	3.1466e-2	0.9989	3.6147e-2	0.9980	4.3198e-2	0.9972	5.1991e-2	0.9967
64	1.4894e-2	0.9998	1.5736e-2	0.9997	1.8079e-2 0	0.9996	2.1608e-2	0.9994	2.6099e-2	0.9993

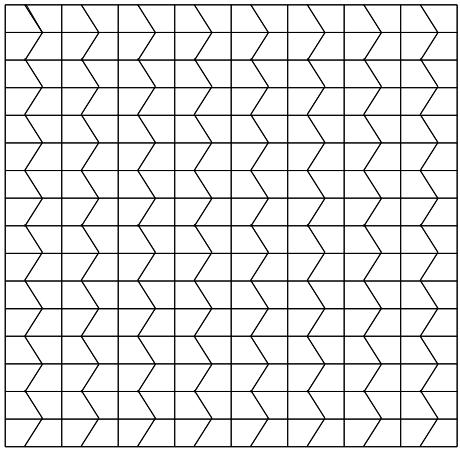

Fig. 5 Nonuniform quadrilateral mesh

Secondly, we apply Q_1-conforming quadrilateral FVM to the test problem (45) based on nonoverlapping control volume (I) and overlapping control volume (II) in Fig. 3, respectively. And then we use Q_1-conforming quadrilateral FEM to the test problem (45). Numerical results on the trapezoidal meshes are presented in Tables 4–6 in terms of the H^1-seminorm convergence rates. In Table 4, we present five cases for $\theta=0$, $\frac{1}{4}$, $\frac{1}{2}$, $\frac{3}{4}$ and 1. We observe from Table 4 that the convergence rates are optimal on these general quadrilateral meshes, which confirm our theoretical analysis. In Tables 5–6, we only present five cases for $\theta=0$, $\frac{1}{32}$, $\frac{1}{16}$, $\frac{1}{8}$ and $\frac{1}{4}$, since numerical results of the last two of these methods are not good as $\theta\geq\frac{1}{4}$. We observe from Tables 5–6 that the convergence rates are not optimal on these

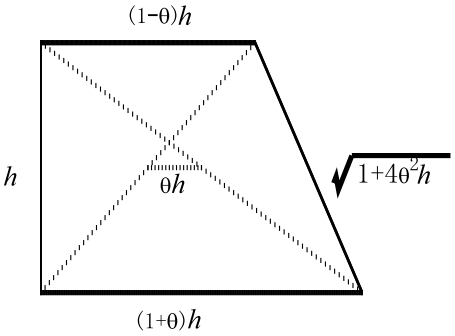

Fig. 6 The shape of quadrilateral element

Table 3 FEM with P_1-nonconforming quadrilateral element

N	$\theta=0$		$\theta=\frac{1}{4}$		$\theta=\frac{1}{2}$		$\theta=\frac{3}{4}$		$\theta=1$	
	$\frac{\lvert u-u_h\rvert}{\lvert u\rvert}$	Rate	$\frac{\lvert u-u_h\rvert}{\lvert u\rvert}$	Rate	$\frac{\lvert u-u_h\rvert}{\lvert u\rvert}$	Rate	$\frac{\lvert u-u_h\rvert}{\lvert u\rvert}$	Rate	$\frac{\lvert u-u_h\rvert}{\lvert u\rvert}$	Rate
4	2.3507e-1	–	2.4638e-1	–	2.7643e-1	–	3.2167e-1	–	3.7855e-1	–
8	1.1876e-1	0.9851	1.2476e-1	0.9817	1.4114e-1	0.9667	1.6708e-1	0.9450	2.0002e-1	0.9204
16	5.9527e-2	0.9964	6.2561e-2	0.9959	7.1067e-2	0.9930	8.4194e-2	0.9888	1.0112e-1	0.9840
32	2.9782e-2	0.9991	3.1302e-2	0.9990	3.5573e-2	0.9984	4.2170e-2	0.9975	5.0685e-2	0.9965
64	1.4894e-2	0.9998	1.5653e-2	0.9999	1.7791e-2	0.9997	2.1093e-2	0.9995	2.5356e-2	0.9992

Table 4 FVM with Q_1-conforming quadrilateral element based on nonoverlapping control volume

N	$\theta=0$		$\theta=\frac{1}{4}$		$\theta=\frac{1}{2}$		$\theta=\frac{3}{4}$		$\theta=1$	
	$\frac{\lvert u-u_h\rvert}{\lvert u\rvert}$	Rate	$\frac{\lvert u-u_h\rvert}{\lvert u\rvert}$	Rate	$\frac{\lvert u-u_h\rvert}{\lvert u\rvert}$	Rate	$\frac{\lvert u-u_h\rvert}{\lvert u\rvert}$	Rate	$\frac{\lvert u-u_h\rvert}{\lvert u\rvert}$	Rate
4	1.7619e-1	–	1.8098e-1	–	1.9647e-1	–	2.2359e-1	–	2.5768e-1	–
8	8.7787e-2	1.0051	9.0160e-2	1.0046	9.7879e-2	1.0052	1.0988e-1	1.0249	1.2303e-1	1.0666
16	4.3856e-2	1.0012	4.5036e-2	1.0014	4.8874e-2	1.0019	5.4672e-2	1.0071	6.0756e-2	1.0179
32	2.1923e-2	1.0003	2.2512e-2	1.0004	2.4428e-2	1.0005	2.7302e-2	1.0018	3.0283e-2	1.0045
64	1.0961e-2	1.0001	1.1255e-2	1.0001	1.2213e-2	1.0001	1.3647e-2	1.0005	1.5130e-2	1.0011

general quadrilateral meshes and decrease as θ increases. Furthermore, the relatively errors $\frac{|u-u_h|}{|u|}$ of three methods by using Q_1-conforming quadrilateral element increase similarly as θ increases, respectively.

Thirdly, we present numerical results in Tables 7–12 in terms of the L^2-norm convergence rates. We observe from these tables that the convergence rates are optimal on these general quadrilateral meshes only for P_1-nonconforming quadrilateral FVM based on nonoverlapping control volume (I) and overlapping control volume (II) and P_1-nonconforming quadrilateral FEM, and Q_1-conforming quadrilateral FVM based on nonoverlapping control volume (I). For other two methods, we can not obtain good numerical results as $\theta \geq \frac{1}{4}$ in Tables 11–12. The convergence rates of the last two of these methods decrease as θ increases. Furthermore the relatively errors $\frac{\|u-u_h\|_0}{\|u\|_0}$ of six methods by using P_1-nonconforming quadrilateral element and Q_1-conforming quadrilateral element increase as θ increases, respectively. Moreover, we find that the results of FVE (or FEM)

Table 5 FVM with Q_1-conforming quadrilateral element based on overlapping control volume

N	$\theta=0$		$\theta=\frac{1}{32}$		$\theta=\frac{1}{16}$		$\theta=\frac{1}{8}$		$\theta=\frac{1}{4}$	
	$\frac{\lvert u-u_h\rvert}{\lvert u\rvert}$	Rate	$\frac{\lvert u-u_h\rvert}{\lvert u\rvert}$	Rate	$\frac{\lvert u-u_h\rvert}{\lvert u\rvert}$	Rate	$\frac{\lvert u-u_h\rvert}{\lvert u\rvert}$	Rate	$\frac{\lvert u-u_h\rvert}{\lvert u\rvert}$	Rate
4	1.8057e-1	–	1.8066e-1	–	1.8079e-1	–	1.8131e-1	–	1.8409e-1	–
8	8.8289e-2	1.0322	8.8331e-2	1.0322	8.8439e-2	1.0316	8.8872e-2	1.0286	9.0863e-2	1.0187
16	4.3917e-2	1.0075	4.3940e-2	1.0074	4.4005e-2	1.0070	4.4275e-2	1.0052	4.5468e-2	0.9988
32	2.1931e-2	1.0018	2.1949e-2	1.0014	2.2002e-2	1.0000	2.2220e-2	0.9946	2.3129e-2	0.9752
64	1.0962e-2	1.0005	1.0985e-2	0.9986	1.1053e-2	0.9932	1.1324e-2	0.9752	1.2362e-2	0.9038

Table 6 FEM with Q_1-conforming quadrilateral element

N	$\theta=0$		$\theta=\frac{1}{32}$		$\theta=\frac{1}{16}$		$\theta=\frac{1}{8}$		$\theta=\frac{1}{4}$	
	$\frac{\lvert u-u_h\rvert}{\lvert u\rvert}$	Rate	$\frac{\lvert u-u_h\rvert}{\lvert u\rvert}$	Rate	$\frac{\lvert u-u_h\rvert}{\lvert u\rvert}$	Rate	$\frac{\lvert u-u_h\rvert}{\lvert u\rvert}$	Rate	$\frac{\lvert u-u_h\rvert}{\lvert u\rvert}$	Rate
4	1.7619e-1	–	1.7644e-1	–	1.7706e-1	–	1.7943e-1	–	1.8889e-1	–
8	8.7787e-2	1.0051	8.8356e-2	0.9978	9.0019e-2	0.9760	9.6322e-2	0.8974	1.1765e-1	0.6830
16	4.3855e-2	1.0012	4.5287e-2	0.9642	4.9318e-2	0.8681	6.2742e-2	0.6184	0.9820e-2	0.2607
32	2.1923e-2	1.0003	2.5044e-2	0.8570	3.2512e-2	0.6015	5.2512e-2	0.2568	0.9571e-2	0.3711
64	1.0961e-2	1.0001	1.6541e-2	0.5960	2.7056e-2	0.2650	5.0358e-2	0.0604	0.9649e-2	−0.012

Table 7 FVM with P_1-nonconforming quadrilateral element based on nonoverlapping control volume

N	$\theta=0$		$\theta=\frac{1}{4}$		$\theta=\frac{1}{2}$		$\theta=\frac{3}{4}$		$\theta=1$	
	$\frac{\lvert u-u_h\rvert}{\lvert u\rvert}$	Rate	$\frac{\lvert u-u_h\rvert}{\lvert u\rvert}$	Rate	$\frac{\lvert u-u_h\rvert}{\lvert u\rvert}$	Rate	$\frac{\lvert u-u_h\rvert}{\lvert u\rvert}$	Rate	$\frac{\lvert u-u_h\rvert}{\lvert u\rvert}$	Rate
4	6.5202e-2	–	7.5280e-2	–	1.0452e-1	–	1.6836e-1	–	2.6297e-1	–
8	1.6180e-2	2.0107	1.9475e-2	1.9506	2.9217e-2	1.8388	4.9105e-2	1.7776	7.8978e-2	1.7354
16	4.0630e-3	1.9936	4.9271e-3	1.9828	7.5049e-3	1.9609	1.2756e-2	1.9447	2.0766e-2	1.9272
32	1.0460e-3	1.9576	1.2487e-3	1.9803	1.8770e-3	1.9994	3.9140e-3	1.9977	5.2293e-3	1.9896
64	2.9930e-4	1.8503	3.3409e-4	1.9023	4.6295e-4	2.0195	7.7547e-4	2.0422	1.2796e-3	2.0309

Table 8 FVM with P_1-nonconforming quadrilateral element based on overlapping control volume

N	$\theta=0$		$\theta=\frac{1}{4}$		$\theta=\frac{1}{2}$		$\theta=\frac{3}{4}$		$\theta=1$	
	$\frac{\lvert u-u_h\rvert}{\lvert u\rvert}$	Rate	$\frac{\lvert u-u_h\rvert}{\lvert u\rvert}$	Rate	$\frac{\lvert u-u_h\rvert}{\lvert u\rvert}$	Rate	$\frac{\lvert u-u_h\rvert}{\lvert u\rvert}$	Rate	$\frac{\lvert u-u_h\rvert}{\lvert u\rvert}$	Rate
4	5.8302e-2	–	7.6605e-2	–	1.2680e-1	–	2.1466e-1	–	3.3036e-1	–
8	1.4740e-2	1.9839	2.0596e-2	1.8951	3.7260e-2	1.7669	6.6243e-2	1.6962	1.0586e-1	1.6419
16	3.6962e-3	1.9956	5.2518e-3	1.9715	9.7184e-3	1.9388	1.7528e-2	1.9181	2.8414e-2	1.8975
32	9.2977e-4	1.9911	1.3079e-3	2.0056	2.4262e-3	2.0020	4.4100e-3	1.9908	7.1993e-3	1.9807
64	2.4837e-4	1.9044	3.2265e-4	2.0192	5.7964e-4	2.0655	1.0687e-3	2.0449	1.7676e-3	2.0261

with P_1-nonconforming quadrilateral element are similar to the results of FVE with Q_1-conforming quadrilateral element. As expected, the errors become smaller as the meshes are refined.

Table 9 FEM with P_1-nonconforming quadrilateral element

N	$\theta=0$		$\theta=\frac{1}{4}$		$\theta=\frac{1}{2}$		$\theta=\frac{3}{4}$		$\theta=1$	
	$\frac{\lvert u-u_h\rvert}{\lvert u\rvert}$	Rate	$\frac{\lvert u-u_h\rvert}{\lvert u\rvert}$	Rate	$\frac{\lvert u-u_h\rvert}{\lvert u\rvert}$	Rate	$\frac{\lvert u-u_h\rvert}{\lvert u\rvert}$	Rate	$\frac{\lvert u-u_h\rvert}{\lvert u\rvert}$	Rate
4	5.8301e-2	–	7.4998e-2	–	1.1518e-1	–	1.8540e-1	–	2.8177e-1	–
8	1.4740e-2	1.9839	1.9843e-2	1.9182	3.2922e-2	1.8067	5.5775e-2	1.7330	8.8058e-2	1.6780
16	3.6962e-3	1.9956	5.0363e-3	1.9782	8.5216e-3	1.9491	1.4663e-2	1.9274	2.3488e-2	1.9066
32	9.2977e-4	1.9911	1.2558e-3	2.0038	2.1273e-3	2.0028	3.6834e-3	1.9931	5.9380e-3	1.9838
64	2.4837e-4	1.9044	3.1321e-4	2.0034	5.1284e-4	2.0525	8.9529e-4	2.0406	1.4541e-3	2.0298

Table 10 FVM with Q_1-conforming quadrilateral element based on nonoverlapping control volume

N	$\theta=0$		$\theta=\frac{1}{4}$		$\theta=\frac{1}{2}$		$\theta=\frac{3}{4}$		$\theta=1$	
	$\frac{\lvert u-u_h\rvert}{\lvert u\rvert}$	Rate	$\frac{\lvert u-u_h\rvert}{\lvert u\rvert}$	Rate	$\frac{\lvert u-u_h\rvert}{\lvert u\rvert}$	Rate	$\frac{\lvert u-u_h\rvert}{\lvert u\rvert}$	Rate	$\frac{\lvert u-u_h\rvert}{\lvert u\rvert}$	Rate
4	5.1254e-2	–	6.5901e-2	–	9.2076e-2	–	1.2492e-1	–	1.6231e-1	–
8	1.2510e-2	2.0345	1.5988e-2	2.0433	2.2080e-2	2.0601	2.9670e-2	2.0739	3.8447e-2	2.0778
16	3.1072e-3	2.0095	3.9642e-3	2.0119	5.4567e-3	2.0166	7.3133e-3	2.0204	9.4783e-3	2.0202
32	7.7549e-4	2.0024	9.8897e-4	2.0030	1.3602e-3	2.0042	1.8222e-3	2.0048	2.3636e-3	2.0036
64	1.9379e-4	2.0006	2.4711e-4	2.0008	3.3982e-4	2.0010	4.5525e-4	2.0010	5.9080e-4	2.0002

Table 11 FVM with Q_1-conforming quadrilateral element based on overlapping control volume

N	$\theta=0$		$\theta=\frac{1}{32}$		$\theta=\frac{1}{16}$		$\theta=\frac{3}{8}$		$\theta=\frac{1}{4}$	
	$\frac{\lvert u-u_h\rvert}{\lvert u\rvert}$	Rate	$\frac{\lvert u-u_h\rvert}{\lvert u\rvert}$	Rate	$\frac{\lvert u-u_h\rvert}{\lvert u\rvert}$	Rate	$\frac{\lvert u-u_h\rvert}{\lvert u\rvert}$	Rate	$\frac{\lvert u-u_h\rvert}{\lvert u\rvert}$	Rate
4	2.7044e-2	–	2.8855e-2	–	3.0713e-2	–	3.4931e-2	–	4.4806e-2	–
8	6.1174e-3	2.1443	6.6195e-3	2.1240	7.1292e-3	2.1071	8.2743e-3	2.0778	1.1753e-2	2.0241
16	1.4482e-3	2.0393	1.6167e-3	2.0337	1.7483e-3	2.0278	2.0696e-3	1.9993	3.2522e-3	1.8536
32	3.6974e-4	2.0101	4.0175e-4	2.0087	4.3988e-4	1.9908	5.9398e-4	1.8009	1.4053e-3	1.2105
64	9.2206e-5	2.0025	1.0136e-4	1.9869	1.2925e-4	1.7669	3.1461e-4	0.9169	1.1162e-3	0.3324

Table 12 FEM with Q_1-conforming quadrilateral element

N	$\theta=0$		$\theta=\frac{1}{32}$		$\theta=\frac{1}{16}$		$\theta=\frac{3}{8}$		$\theta=\frac{1}{4}$	
	$\frac{\lvert u-u_h\rvert}{\lvert u\rvert}$	Rate	$\frac{\lvert u-u_h\rvert}{\lvert u\rvert}$	Rate	$\frac{\lvert u-u_h\rvert}{\lvert u\rvert}$	Rate	$\frac{\lvert u-u_h\rvert}{\lvert u\rvert}$	Rate	$\frac{\lvert u-u_h\rvert}{\lvert u\rvert}$	Rate
4	5.1295e-2	–	5.2526e-2	–	5.4197e-2	–	5.8785e-2	–	7.2364e-2	–
8	1.2705e-2	2.0134	1.2958e-2	2.0192	1.3236e-2	2.0338	1.3959e-2	2.0743	1.7108e-2	2.0806
16	3.1684e-3	2.0036	3.1714e-3	2.0307	3.1400e-3	2.0756	3.9742e-3	1.8124	1.2042e-2	0.5058
32	7.9158e-4	2.0009	7.4859e-4	2.0829	1.0088e-3	1.6381	3.6072e-3	0.1398	1.4301e-2	−0.247
64	1.9786e-4	2.0002	2.5507e-4	1.5533	9.6791e-4	0.0597	3.9956e-3	−0.148	1.5411e-2	−0.108

Finally, we present the superconvergence of derivative of six methods. Here E_{Du} denotes the mean relative error of derivative of u_h at center points of the quadrilateral mesh.

Table 13 Mean relative error of derivative at the central point of partition for P_1-nonconforming quadrilateral FVM with nonoverlapping control volume

N	$\theta=0$		$\theta=\frac{1}{4}$		$\theta=\frac{1}{2}$		$\theta=\frac{3}{4}$		$\theta=1$	
	E_{Du}	Rate	E_{Du}	Rate	E_{Du}	Rate	E_{Du}	Rate	E_{Du}	Rate
4	4.6618e-2	–	1.2343e-1	–	2.0473e-1	–	2.8420e-1	–	3.5022e-1	–
8	1.4235e-2	1.7115	5.8244e-2	1.0835	1.0955e-1	0.9021	1.5158e-1	0.9069	1.8451e-1	0.9246
16	3.6987e-3	1.9443	2.9543e-2	0.9793	5.6957e-2	0.9437	7.9237e-2	0.9358	9.5695e-2	0.9472
32	1.0064e-3	1.8778	1.5060e-2	0.9720	2.9259e-2	0.9610	4.0781e-2	0.9583	4.9267e-2	0.9578
64	3.1655e-4	1.6687	7.6500e-3	0.9724	1.4898e-2	0.9738	2.0769e-2	0.9735	2.5099e-2	0.9730

Table 14 Mean relative error of derivative at the central point of partition for P_1-nonconforming quadrilateral FVM with overlapping control volume

N	$\theta=0$		$\theta=\frac{1}{4}$		$\theta=\frac{1}{2}$		$\theta=\frac{3}{4}$		$\theta=1$	
	E_{Du}	Rate	E_{Du}	Rate	E_{Du}	Rate	E_{Du}	Rate	E_{Du}	Rate
4	3.6501e-2	–	9.7746e-2	–	1.6695e-1	–	2.5406e-1	–	3.5997e-1	–
8	9.7271e-3	1.9078	4.8802e-2	1.0021	9.1540e-2	0.8670	1.2803e-1	0.9887	1.6610e-1	1.1158
16	2.5840e-3	1.9124	2.5446e-2	0.9395	4.7608e-2	0.9432	6.4667e-2	0.9854	8.1747e-2	1.0228
32	7.1634e-4	1.8509	1.3003e-2	0.9686	2.4361e-2	0.9666	3.2829e-2	0.9781	4.1281e-2	0.9857
64	2.3768e-4	1.5916	6.5917e-3	0.9801	1.2372e-2	0.9775	1.6626e-2	0.9816	2.0903e-2	0.9818

Table 15 Mean relative error of derivative at the central point of partition for P_1-nonconforming quadrilateral FEM

N	$\theta=0$		$\theta=\frac{1}{4}$		$\theta=\frac{1}{2}$		$\theta=\frac{3}{4}$		$\theta=1$	
	E_{Du}	Rate	E_{Du}	Rate	E_{Du}	Rate	E_{Du}	Rate	E_{Du}	Rate
4	3.6486e-2	–	1.0352e-1	–	1.7815e-1	–	2.4520e-1	–	3.1933e-1	–
8	9.7252e-3	1.9076	5.3475e-2	0.9529	1.0143e-1	0.8126	1.3970e-1	0.8116	1.6787e-1	0.9274
16	2.5839e-3	1.9122	2.7949e-2	0.9361	5.3409e-2	0.9253	7.3343e-2	0.9296	8.7808e-2	0.9349
32	7.1634e-4	1.8509	1.4321e-2	0.9647	2.7516e-2	0.9568	3.7843e-2	0.9546	4.5191e-2	0.9883
64	2.3768e-4	1.5916	7.2834e-3	0.9754	1.4015e-2	0.9733	1.9274e-2	0.9733	2.3006e-2	0.9740

Numerical results of the superconvergence of derivative are presented in Tables 13–16. We observe from these tables that the superconvergence points of derivative exist if and only if $\theta = 0$ for these methods. For other cases, there are no similar superconvergences at the nodes of the partition and the midpoints of edges. Furthermore, we can obtain better convergence of derivative of u_h at center points as θ increases for P_1-nonconforming quadrilateral FVM and P_1-nonconforming quadrilateral FEM, and Q_1-conforming quadrilateral FVM with nonoverlapping control volume. On the other hand, we can observe that numerical results are not good as $\theta \geq \frac{1}{4}$ in Tables 17–18 for other two methods.

Remark 6.1 The smallness of the quantity d_τ is a good indicator of almost parallelogram. From Fig. 6, we obtain the midpoints distance $d_\tau = \theta h$. On one hand, if $\theta = o(h)$, i.e., $d_\tau = o(h^2)$ satisfies the usual Bi-section condition [20], we can obtain good numerical results. On the other hand, if $\theta \to 0$, i.e., $d_\tau \to 0$, then we have good numerical results similarly. In a

Table 16 Mean relative error of derivative at the central point of partition for Q_1-conforming quadrilateral FVM with nonoverlapping control volume

N	$\theta=0$		$\theta=\frac{1}{4}$		$\theta=\frac{1}{2}$		$\theta=\frac{3}{4}$		$\theta=1$	
	E_{Du}	Rate	E_{Du}	Rate	E_{Du}	Rate	E_{Du}	Rate	E_{Du}	Rate
4	4.3958e-2	–	9.6325e-2	–	1.7191e-1		2.3491e-1	–	2.7949e-1	–
8	1.1518e-2	1.9323	4.6292e-2	1.0572	8.9263e-2	0.9455	1.2368e-1	0.9255	1.4710e-1	0.9260
16	3.0116e-3	1.9353	2.2976e-2	1.0106	4.5761e-2	0.9640	6.3831e-2	0.9543	7.6020e-2	0.9523
32	7.7410e-4	1.9599	1.1525e-2	0.9954	2.3302e-2	0.9736	3.2578e-2	0.9704	3.8825e-2	0.9694
64	1.9652e-4	1.9779	5.8262e-3	0.9841	1.1849e-2	0.9754	1.6580e-2	0.9744	1.9764e-2	0.9741

Table 17 Mean relative error of derivative at the central point of partition for Q_1-conforming quadrilateral FVM with overlapping control volume

N	$\theta=0$		$\theta=\frac{1}{32}$		$\theta=\frac{1}{16}$		$\theta=\frac{1}{8}$		$\theta=\frac{1}{4}$	
	E_{Du}	Rate	E_{Du}	Rate	E_{Du}	Rate	E_{Du}	Rate	E_{Du}	Rate
4	3.6645e-2	–	3.7460e-2	–	4.3507e-2	–	5.8696e-2	–	9.4814e-2	–
8	9.6639e-3	1.9151	1.2052e-2	1.6361	1.5943e-2	1.4483	2.5579e-2	1.1983	4.8917e-2	0.9548
16	2.5188e-3	1.9398	4.1869e-3	1.5253	6.5071e-3	1.2928	1.2045e-2	1.0865	2.5289e-2	0.9518
32	6.4923e-4	1.9160	1.6473e-3	1.3458	2.9344e-3	1.1490	5.9721e-3	1.0121	1.2916e-2	0.9694
64	1.6522e-4	1.9744	7.2941e-4	1.1753	1.4277e-3	1.0393	3.0379e-3	0.9752	6.7100e-3	0.9448

Table 18 Mean relative error of derivative at the central point of partition for Q_1-conforming quadrilateral FEM

N	$\theta=0$		$\theta=\frac{1}{32}$		$\theta=\frac{1}{16}$		$\theta=\frac{1}{8}$		$\theta=\frac{1}{4}$	
	E_{Du}	Rate	E_{Du}	Rate	E_{Du}	Rate	E_{Du}	Rate	E_{Du}	Rate
4	4.4148e-2	–	4.7424e-2	–	5.4727e-2	–	7.8010e-2	–	1.1311e-1	–
8	1.1793e-3	1.9044	1.6687e-2	1.5069	2.4987e-2	1.1311	4.5375e-2	0.7818	8.9740e-2	0.5469
16	3.0952e-3	1.9298	7.4370e-3	1.1660	1.3944e-2	0.8415	2.8542e-2	0.6688	6.1612e-2	0.5425
32	7.9596e-4	1.9593	3.8950e-3	0.9331	8.0240e-3	0.7972	1.7908e-2	0.6724	4.4086e-2	0.4829
64	2.0204e-4	1.9780	2.1575e-3	0.8523	4.8484e-3	0.7268	1.2367e-2	0.5341	3.6057e-2	0.2900

word, the convergence rate of the P_1-nonconforming quadrilateral element is independent of the mesh distortion parameter θ. These numerical results coincide with the theoretical results.

Remark 6.2 In 2005, Hu and Shi [20] defined a constrained nonconforming rotated Q_1-element (CNR-Q_1) and analyzed the superconvergence of the CNR-Q_1 element for the linear elliptic problems. They pointed out the CNR-Q_1 element is equivalent to the P_1-nonconforming element [34] on the rectangle mesh. They have the same properties on the rectangle mesh. For the general quadrilateral mesh, it is still unknown whether there are similar results. From numerical experiments in [20], we know the relative errors of P_1-nonconforming quadrilateral element is smallest on the general quadrilateral mesh for Poisson equation, and the convergence rate of P_1-nonconforming element is independent of the

mesh distortion parameter. From Tables 1–18, we can obtain the similar numerical laws for the semilinear elliptic problems by P_1-nonconforming quadrilateral element.

Remark 6.3 Recently, Mao et al. give a more general framework to construct effective FEM by using the different ideas, and novel DSP element and QB element are proposed in [29, 31, 32]. In fact, QB element is equivalent to the nonparametic P_1-nonconforming quadrilateral element [34] under rectangular meshes, but for general quadrilateral meshes, they are not equivalent. Moreover, the nonparametic P_1-nonconforming quadrilateral element has the optimal convergence without the Bi-section condition on the meshes and it can be implemented easily.

Remark 6.4 In our numerical experiments, the number of unknown variables is same for every method. And the number of nonzero elements of the coefficient matrix is the least by using P_1-nonconforming element. Each line has at most five nonzero elements by using P_1-nonconforming element and at most nine nonzero elements by using Q_1-conforming element on the rectangle mesh. For other cases, each line of the coefficient matrix has at most nine nonzero elements by using P_1-nonconforming element and Q_1-conforming element respectively.

7 Conclusions

In conclusion, P_1-nonconforming quadrilateral element is a simple and stable element. Numerical analysis and examples have demonstrated excellent stability and convergence properties of the nonconforming FEM and FVM by using the nonoverlapping control volumes and overlapping control volumes, respectively. Moreover, P_1-nonconforming quadrilateral element has better convergence of derivative.

Acknowledgements The authors are very thankful to the anonymous referee who meticulously read through the paper, made many helpful discussions and corrections of the English and typesetting mistakes. This work is in part supported by the National Natural Science Foundation of China (No. 10971166, No. 10901131, No. 61163027), the National High Technology Research and Development Program of China (863 Program, No. 2009AA01A135), the China Postdoctoral Science Foundation (No. 201104702, No. 200801448), and the Natural Science Foundation of Xinjiang Province (No. 2010211B04).

References

1. Acosta, G., Duran, R.: Error estimates for Q_1 isoparametric elements satisfying a weak angle condition. SIAM J. Numer. Anal. **38**(4), 1073–1088 (2000)
2. Bank, R.E., Rose, D.J.: Some error estimates for the box methods. SIAM J. Numer. Anal. **24**(4), 777–787 (1987)
3. Bramble, J.H.: A second-order finite difference analog of the first biharmonia boundary value problem. Numer. Math. **9**(4), 236–249 (1996)
4. Cai, Z.Q.: On the finite volume element method. Numer. Math. **58**, 713–735 (1991)
5. Chatzipantelidis, P.: Finite volume methods for elliptic PDE's: a new approach. Math. Model. Numer. Anal. **3**, 307–324 (2002)
6. Chatzipantelidis, P., Ginting, V., Lazarov, R.D.: A finite volume element method for a nonlinear elliptic problem. Numer. Linear Algebra Appl. **12**(5), 515–545 (2005)
7. Chen, C.M., Huang, Y.Q.: High Accuracy Theory of Finite Element Methods. Hunan Science, Changsha (1995). (in Chinese)
8. Chen, C.M., Larson, S., Zhang, N.Y.: Error estimates of optimal order for finite element methods interpolated coefficients for the nonlinear heat equation. IMA J. Numer. Anal. **9**, 507–524 (1989)

9. Chen, L.: A new class of high order finite volume methods for second order elliptic equations. SIAM J. Numer. Anal. **47**(6), 4021–4043 (2010)
10. Chou, S.H.: Analysis and convergence of a covolume method for the generalized Stokes problem. Math. Comput. **66**, 85–104 (1997)
11. Chou, S.H., He, S.N.: On the regularity and uniformness conditions on quadrilateral grids. Comput. Methods Appl. Mech. Eng. **191**, 5149–5158 (2002)
12. Chou, S.H., Kwak, D.Y., Kim, K.Y.: A general framework for constructing and analyzing mixed finite volume methods on quadrilateral grids: The overlapping covolume case. SIAM J. Numer. Anal. **39**(4), 1170–1196 (2001)
13. Duran, R., Lombardi, A.: Error estimates on anisotropic Q_1 elements for functions in weighted Sobolev spaces. Math. Comput. **74**(252), 1679–1706 (2005)
14. El Alaoui, L.: An adaptive finite volume box scheme for solving a class of nonlinear parabolic equations. Appl. Math. Lett. **22**, 291–296 (2009)
15. Eymard, R., Gallouet, T., Herbin, R.: Finite Volume Methods. In: Handbook of Numerical Analysis VII, pp. 713–1020. North-Holland, Amsterdam (2000)
16. Feng, X.L., Kim, I., Nam, H., Sheen, D.: Locally stabilized P_1-nonconforming quadrilateral and hexahedral finite element method for the Stokes equations. J. Comput. Appl. Math. **236**(5), 714–727 (2011)
17. Frehse, J., Rannacher, R.: Asymptotic L^∞-error estimate for linear finite element approximations of quasilinear boundary value problems. SIAM J. Numer. Anal. **15**, 418–431 (1978)
18. Grajewski, M., Hron, J., Turek, S.: Numerical analysis for a new nonconforming linear finite element on quadrilaterals. J. Comput. Appl. Math. **193**, 38–50 (2006)
19. He, Y.N., Feng, X.L.: H^1-stability and convergence of the FE, FD and FV methods for the Poisson equation. Preprint
20. Hu, J., Shi, Z.C.: Constrained quadrilateral nonconforming rotated Q_1 element. J. Comput. Math. **23**(5), 561–586 (2005)
21. Lamichhane, B.P.: Inf-sup stable finite-element pairs based on dual meshes and bases for nearly incompressible elasticity. IMA J. Numer. Anal. **29**, 404–420 (2009)
22. Larson, S., Thomee, V., Zhang, N.Y.: Interpolation of coefficients and transformation of dependent variable in element methods for the nonlinear heat equation. Math. Methods Appl. Sci. **11**, 105–124 (1989)
23. Li, R.H., Chen, Z., Wu, W.: Generalized Difference Methods for Differential Equations: Numerical Analysis of Finite Volume Methods. Marcel Dekker, New York (2000)
24. Li, Y.H., Li, R.H.: Generalized difference methods on arbitrary quadrilateral networks. J. Comput. Math. **17**, 653–672 (1999)
25. Liu, H.P., Yan, N.N.: Superconvergence analysis of the nonconforming quadrilateral linear-constant scheme for Stokes equations. Adv. Comput. Math. **29**, 375–392 (2008)
26. Lv, J.L., Li, Y.H.: L^2 error estimate of the finite volume element methods on quadrilateral meshes. Adv. Comput. Math. **33**, 129–148 (2010)
27. Man, H.Y., Shi, Z.C.: P_1-nonconforming quadrilateral finite volume element method and its cascadic multigrid algorithm. J. Comput. Math. **24**, 59–80 (2006)
28. Mao, S.P., Chen, S.C.: A new nonconforming double set parameter finite element. In: Proceedings of the Seventh China-Japan Seminar on Numerical Mathematics, ZhangjiaJie (2004)
29. Mao, S.P., Chen, S.C.: A quadrilateral nonconforming finite element for linear elasticity problem. Adv. Comput. Math. **28**, 81–100 (2008)
30. Mao, S.P., Chen, S.C.: Convergence and superconvergence of a non-conforming finite element for Stokes problem. J. Numer. Math. **14**, 83–101 (2006)
31. Mao, S.P., Chen, S.C., Sun, H.X.: A quadrilateral, anisotropic, superconvergent nonconforming double set parameter element. Appl. Numer. Math. **56**, 937–961 (2006)
32. Mao, S.P., Nicaise, S., Shi, Z.C.: On the interpolation error estimates for Q_1 quadrilateral finite elements. SIAM J. Numer. Anal. **47**(1), 467–486 (2008)
33. Park, C.: A study on locking phenomena in finite element methods. Ph.D. thesis, Department of Mathematics, Seoul National University, Seoul, Korea (2002). Available at http://www.nasc.snu.ac.kr/cpark/papers/phdthesis.ps.gz
34. Park, C., Sheen, D.: P_1-nonconforming quadrilateral finite element methods for second-order elliptic problems. SIAM J. Numer. Anal. **41**(2), 624–640 (2003)
35. Schmidt Kiel, T.: Box schemes on quadrilateral meshes. Computing **51**, 271–292 (1993)
36. Wang, T.K.: A mixed finite volume element method based on rectangular mesh for biharmonic equations. J. Comput. Appl. Math. **172**, 117–130 (2004)
37. Xiong, Z.G., Chen, C.M.: Superconvergence of triangular quadratic finite element method with interpolated coefficients for nonlinear elliptic problem. Acta Math. Sci. Ser., **26**(2), 174–182 (2006). (in Chinese)

38. Xiong, Z.G., Chen, C.M.: Superconvergence of rectangular finite element with interpolated coefficients for semilinear elliptic problem. Appl. Math. Comput. **181**, 1577–1584 (2006)
39. Xiong, Z.G., Chen, C.M.: Superconvergence of continuous finite elements with interpolated coefficients for initial value problems of nonlinear ordinary differential equation. Numer. Math. J. Chin. Univ. **16**(1), 37–44 (2007)
40. Xiong, Z.G., Chen, Y.P.: A rectangular finite volume element method for a semilinear elliptic equation. J. Sci. Comput. **36**, 177–191 (2008)
41. Xiong, Z.G., Chen, Y.P.: Finite volume element method with interpolated coefficients for two-point boundary value problem of semilinear differential equations. Comput. Methods Appl. Mech. Eng. **196**, 3798–3804 (2007)
42. Xu, J.C., Zou, Q.S.: Analysis of linear and quadratic simplicial finite volume methods for elliptic equations. Numer. Math. **111**(3), 469–492 (2009)
43. Yang, M.: A second-order finite volume element method on quadrilateral meshes for elliptic equations. Modél. Math. Anal. Numér. **40**(6), 1053–1067 (2006)
44. Zhang, H.Q., Wang, M.: The Mathematical Theory of Finite Elements. Science Press, Beijing (1991). (in Chinese)
45. Zhu, P., Li, R.H.: Generalized difference methods for second order elliptic partial differential equations (II)-quadrilateral grids. Numer. Math. J. Chin. Univ. **4**, 360–375 (1982)
46. Zlamal, M.: A finite element solution of the nonlinear heat equation. RAIRO Model. Anal. Numer **14**, 203–216 (1980)